

pubs.acs.org/JPCL Letter

# Direct Measurement of Intermolecular Mechanical Force for Nonspecific Interactions between Small Molecules

3 Shankar Pandey, Yuan Xiang, Dirk Friedrich, Yongsheng Leng, and Hanbin Mao\*



Cite This: https://doi.org/10.1021/acs.jpclett.1c03142



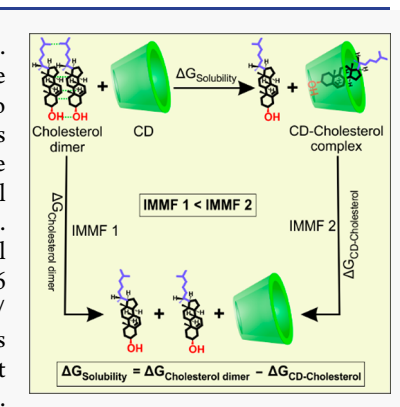
**ACCESS** I

Metrics & More

Article Recommendations

s Supporting Information

4 **ABSTRACT:** Mechanical force can evaluate intramolecular interactions in macromolecules. 5 Because of the rapid motion of small molecules, it is extremely challenging to measure 6 mechanical forces of nonspecific intermolecular interactions. Here, we used optical tweezers to 7 directly examine the intermolecular mechanical force (IMMF) of nonspecific interactions 8 between two cholesterols. We found that IMMFs of dimeric cholesterol complexes were 9 dependent on the orientation of the interaction. The surprisingly high IMMF in cholesterol 10 dimers ( $\sim$ 30 pN) is comparable to the mechanical stability of DNA secondary structures. 11 Using Hess-like cycles, we quantified that changes in free energy of solubilizing cholesterol 12 ( $\Delta G_{\text{solubility}}$ ) by  $\beta$ -cyclodextrin ( $\beta$ CD) and methylated  $\beta$ CD (Me- $\beta$ CD) were as low as -16 13 and -27 kcal/mol, respectively. Compared to the  $\Delta G_{\text{solubility}}$  of cholesterols in water (5.1 kcal/14 mol), these values indicated that cyclodextrins can easily solubilize cholesterols. Our results 15 demonstrated that the IMMF can serve as a generic and multipurpose variable to dissect 16 nonspecific intermolecular interactions among small molecules into orientational components.



When two molecules interact with each other, intermolecular force (IMF)<sup>2</sup> is used to evaluate the strength
of the interaction. IMF can be quantified by chemical energy,
which offers a convenient way to directly compare different
types of IMF. However, as a thermodynamic variable, chemical
energy is pathway independent and cannot probe the
directionality of molecular interactions. Both pathway and
directionality, however, are essential factors to render a full
picture of kinetic intermolecular interactions. For example,
folding or unfolding energy trajectories of proteins are
dependent on the direction of a process in which intermediates
with different local energy minima are located.

Mechanical force is a kinetic variable that is dependent on 30 both pathway and direction of a process.<sup>3,4</sup> Recent technical 31 advances on the application and measurement of picoNewton 32 forces<sup>5</sup> are instrumental to the development of interdisciplinary 33 fields, such as mechanobiology<sup>6-8</sup> and mechanochemistry,<sup>9,10</sup> 34 in which mechanical forces participate in biology and 35 chemistry processes, respectively. Many mechanical properties 36 of polymers and biomacromolecules, such as proteins and 37 nucleic acids, have been portrayed by single molecule force 38 spectroscopy (SMFS)<sup>11–13</sup> in optical tweezers, magnetic 39 tweezers, or AFM instrument. 11 However, almost all measure-40 ments are focused on the intramolecular interactions inside a 41 particular molecule. It is rare to follow intermolecular 42 interactions from a mechanical perspective. 14 It is even more 43 challenging to investigate the mechanochemistry between two 44 small molecules which have large freedom of motion. One 45 reason for this difficulty is the low throughput of the SMFS. It 46 is difficult to repeatedly probe the interaction between two 47 small molecules. Upon dissociation of the two interacting

molecules, it is time-consuming to locate and track the next 48 pair of molecules for measurement. In addition, once two 49 molecules are forced apart, it is almost impossible to evaluate 50 the same molecule pair again, which increases the measure-51 ment noise due to the stochastic variation in consecutive 52 sampling practice.

Our recent success in the investigation of individual host— 54 guest pairs has provided a solution to increase the throughput 55 of SMFS and to address the issue of the variation in stochastic 56 sampling. This has been achieved by introducing a linker 57 between two interacting molecules so that the two components 58 do not escape to the surroundings after mechanical 59 dissociation. As a result, the same molecular pair can 60 repeatedly form an interacting complex for the next round of 61 measurement on a single-molecule platform.

In this work, this strategy has been catapulted to probe the 63 intermolecular mechanical force (IMMF)<sup>15</sup> during the 64 interaction of two cholesterol molecules. As a small molecule, 65 cholesterol is an essential constituent of cell membrane and a 66 precursor for many important biomolecules such as cortico-67 steroids hormone, sex hormones, and vitamin D.<sup>16,17</sup> 68 Cholesterol contains a large hydrophobic motif (central planar 69 fused rings and a flexible hydrocarbon tail, see Figure 1) and a 70 fl

Received: September 24, 2021 Accepted: November 11, 2021



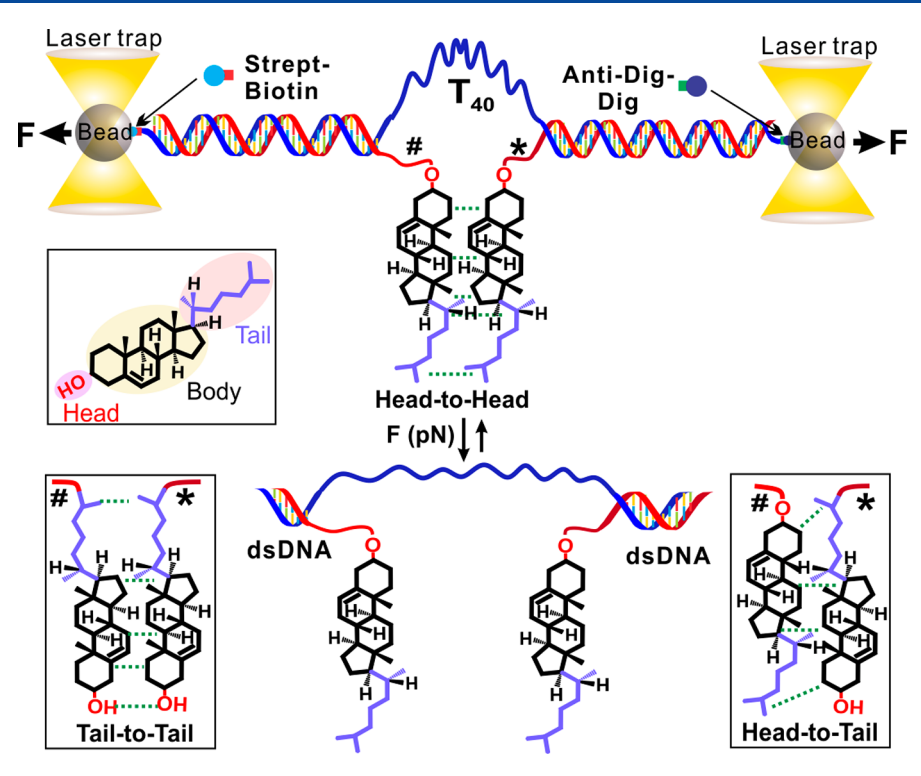


Figure 1. Schematic diagram for single molecular mechanical unfolding of cholesterol dimers with different orientations (bottom insets). The self-assembled construct is sandwiched between two dsDNA handles, which are tethered between two optically trapped polystyrene beads by streptavidin (strep)/biotin and digoxigenin (dig)/antidigoxigenin (anti-dig) interactions. Cholesterol structure is shown in the top inset.

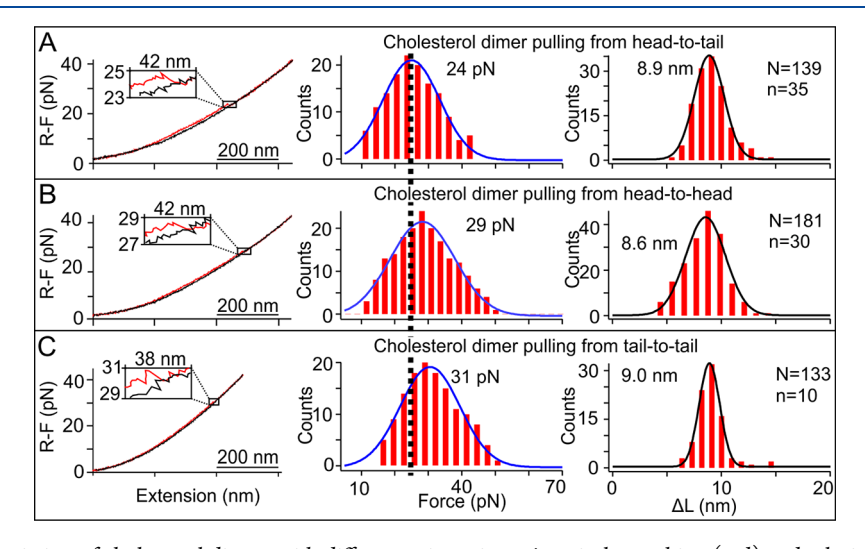


Figure 2. Mechanical dissociation of cholesterol dimers with different orientations. A typical stretching (red) and relaxing (black) force—extension curve, rupture force (IMMF) histogram, and change-in-contour-length ( $\Delta L$ ) histogram for a cholesterol dimer pulled from (A) head-to-tail direction, (B) head-to-head direction, and (C) tail-to-tail direction. The dotted line in the middle panel depicts 24 pN. N and n represent the total numbers of data points and molecules, respectively, for each experiment. The histograms are fitted by Gaussian curves. See SI Figure S15 for fitting based on the equation proposed by Dudko.  $^1$ 

small hydrophilic motif (the hydroxyl headgroup). The central hydrophobic rings have two faces: a flat and smooth face that has no substituents (the  $\alpha$  face) and a rough face with methyl groups (the  $\beta$  face). Owing to its structural complexity, cholesterol may form a dimer in which two  $\alpha$  faces interact with each other. Cholesterol dimers play a fundamental role in many functions such as those that occur in the cell membrane. When cholesterol molecules aggregate, the dimer is the simplest unit based on which the cholesterol

crystal may form in artery plaques, which can cause 80 atherosclerosis conditions. 25

Given the importance of cholesterol molecules in various 82 physiological and pathological processes, here we directly 83 measured the IMMF between two interacting cholesterols 84 (dimer) in aqueous buffer by a single-molecule mechanochemical assay in an optical tweezers instrument (Figure 1). Unlike 86 the IMF which is a thermodynamic variable, IMMF provides a 87 mechanical information between cholesterol molecules. This 88 produces an unprecedented perspective on the kinetic aspect 89

90 of small molecule interactions. Surprisingly, we found that the 91 IMMFs between two nonspecifically interacting cholesterol 92 molecules are comparable to the unfolding force of DNA 93 tetraplexes, <sup>26–28</sup> while higher than the unzipping force of DNA 94 duplexes.<sup>29</sup> By uniquely manipulating orientations of individual 95 cholesterol molecules, we further evaluated the mechanical 96 anisotropy in the interaction of the cholesterol dimers. Finally, 97 the changes in free energy of dissociation of cholesterol dimers were compared with those of cholesterol-cyclodextrin 99 complexes. This allowed us to determine, for the first time, 100 the change in free energy of solubility of cholesterol in  $\beta$ -101 cyclodextrin ( $\beta$ CD) or methylated  $\beta$ CD (Me- $\beta$ CD), two 102 compounds widely used to extract cholesterols from cell 103 membranes or artery plaques. This IMMF measurement 104 therefore provides convenient and direct quantification of the 105 fundamental nonspecific intermolecular processes among small 106 molecules.

Based on different cholesterol alignments, a cholesterol 108 dimer can have three possible orientations: head-to-head, 109 head-to-tail, and tail-to-tail (Figure 1). To evaluate the IMMF 110 of cholesterol dimers with these three orientations, we 111 modified cholesterols either at the alkyl tail with an alkyne 112 group or the hydroxyl head extended with an azide group. The 113 modified cholesterol was conjugated to a single-stranded DNA 114 by copper(I) catalyzed cycloaddition reaction (Figures S1-115 S11). 15,30 The conjugate was finally incorporated in our single-116 molecule platform by self-assembly of DNA strands (Figure 1). 117 The platform contained a polythymidine (T<sub>40</sub>) ssDNA linker which helps keep two cholesterols in close proximity even after 119 the dimer is dissociated. This linker facilitated repeated 120 intercholesterol association and dissociation events. The entire 121 molecular setup was anchored to two optically trapped beads 122 by using affinity linkages of streptavidin/biotin and digox-123 igenin/antibody, respectively (Figure 1).

Using this setup, we first evaluated the mechanical stability 125 of the cholesterol dimer with a misaligned orientation. This 126 was achieved by pulling one cholesterol from the hydroxy head 127 and the other cholesterol from the alkyl tail end (Figure 1, 128 inset). Mechanical dissociation and association of cholesterol 129 dimers were carried out by moving one trapped bead away 130 from the other. This process increased tension in the DNA 131 tether, leading to the dissociation of the cholesterol dimer, 132 which was manifested by a sudden rupture event in a force-133 extension (F-X) curve (Figure 2A, left). After mechanical 134 breaking of the cholesterol dimer, one bead was moved toward 135 another, relaxing the tension in the DNA tether. Since two 136 dissociated cholesterol molecules were still in proximity due to 137 the presence of the T<sub>40</sub> linker, the cholesterol pair would 138 interact again for another cycle of dissociation-association 139 experiment. From these repetitive force ramping experiments, we constructed a rupture force histogram (Figure 2A, middle), which revealed an average IMMF of 24 pN for this type of cholesterol dimer orientation. After the cholesterol dimer is 143 dissociated at 24 pN, the T40 linker will be fully stretched, 144 which leads to an extended molecular construct. By calculating 145 the change in the contour length  $(\Delta L)$  due to this extension 146 (Figure 2A, right), we found the  $\Delta L$  value was close to that 147 expected from the release of the T40 linker after breakage of 148 the cholesterol dimer (see SI and Figure S12 for detailed 149 calculation). This suggested that observed rupture events were 150 due to the dissociation of cholesterol dimers at a specific 151 IMMF.

To confirm that the observed IMMF was indeed due to the  $^{152}$  dissociation of two cholesterols, we performed two control  $^{153}$  experiments. In the first control, we incorporated only one tail- $^{154}$  modified cholesterol in the single-molecule platform. In the  $^{155}$  second control, we integrated a head-modified cholesterol in  $^{156}$  our DNA platform. In each control, we did not observe any  $^{157}$  rupture event, suggesting there should be no interaction  $^{158}$  between cholesterol and the DNA template used in the IMMF  $^{159}$  measurement platform. Thereby, the rupture events observed  $^{160}$  in the F-X curves in Figure 2 were indeed dissociations of  $^{161}$  cholesterol dimers.

Next, we changed the association/dissociation of the 163 cholesterol dimer from the head-tail to the head-head 164 orientation. This was achieved by attaching both cholesterols 165 to the IMMF measurement platform via their hydroxy heads 166 (head-to-head) (Figure 1). The rupture force histogram 167 showed an IMMF of 29 pN (Figure 2B), a value higher than 168 the head-to-tail pulling (24 pN). This can be attributed to a 169 better match in molecular shape between two cholesterols for 170 this head-to-head orientation, which increased the interfacial 171 area of the cholesterol dimer associated via hydrophobic 172 interactions. To test this hypothesis, we prepared another 173 construct in which cholesterol dimers are associated and 174 dissociated from the alkyl tails (tail-to-tail) (Figure 1). We 175 found that the average IMMF for this orientation was 31 pN 176 (Figure 2C). This IMMF was again higher than that of the 177 head-to-tail orientation, suggesting that tail-to-tail orientation 178 also had more contact area between two interacting cholesterol 179 molecules than that in the head-to-tail orientation. Such an 180 orientational effect is of high clinical importance since 181 interaction strength among cholesterol molecules can decide 182 how well cholesterol crystals in the artery plaques are dissolved 183 by chemical agents.

To understand the molecular mechanisms of the cholester- 185 ol-cholesterol interactions, we performed molecular dynamic 186 (MD) simulations (see SI for details) on the mechanical 187 dissociation of the three different dimer conformations studied 188 in single-molecule force measurements. All simulations of 189 dimer dissociation were set to be along either in-plane or out- 190 of-plane of the cholesterol  $\alpha$  faces. However, the final rupture 191 conformation shows the strong tendency of dimer dissociation 192 along the in-plane trajectory, except for the misaligned case, 193 signaling this is most likely the lowest energy pathway of the 194 dimer rupture. MD simulations gave two different values of 195 dissociation force,  $\sim 97$  pN and  $\sim 82$  pN for the head-to-head/ 196 tail-to-tail and the head-to-tail orientations, respectively 197 (Figure S16 for the in-plane and Figure S17 for the out-of- 198 plane dissociations). In Figure S16, we showed that the headto-head/tail-to-tail dissociation forces were larger than that of 200 head-to-tail misaligned contact conformation with statistical 201 significance. These results were consistent with the trend of 202 force histograms shown in Figure 2. However, because of the 203 long flexible DNA handles connected to cholesterol dimers, we 204 could not completely exclude the possible misaligned 205 orientations. But it was clear that the majority of dimer 206 conformations upon association followed the aligned orienta- 207 tion. It is noteworthy that MD simulation gave higher force 208 values due to the requirement of a much higher pulling rate 209 (0.002 Å/ps here) used in the field.  $^{15,31-33}$ 

To quantify the contact area in the cholesterol dimer, we 211 counted the number of C and O atoms within 5 Å between the 212 two cholesterol molecules (blue and orange atoms in Figure 213 S17). For the head-to-head/tail-to-tail contact, we counted 40 214

Figure 3. A schematic diagram to determine the change in free energy of solubilization ( $\Delta G_{\text{solubility}}$ ) of cholesterol in the Me- $\beta$ CD or  $\beta$ CD molecule (green barrel) by using a process analogous to the Hess cycle.

215  $\pm$  2 atoms, while in the head-to-tail, we only found 33  $\pm$  4 216 atoms in their contact plane. This result signifies that the 217 contact area in the head-to-tail dimer is smaller than that in the 218 head-to-head or tail-to-tail dimer, while the latter two clearly 219 have more stable  $\alpha-\alpha$  face-to-face contact conformation 220 (Figure S16A). Such a finding explains why the head-to-tail 221 contact often cannot maintain the face-to-face separation (flip/222 rolling separation) during the pulling, leading to a lower 223 dissociation force which is in accordance with the experimental 224 findings.

After measurements of IMMFs in all three cholesterol 225 226 dimers with different orientations, we further evaluated the 227 stability of cholesterol dimers from free energy perspectives. 228 To this end, we calculated the dissociation works of these three 229 cholesterol dimers, from which changes in free energy of 230 dissociation ( $\Delta G_{
m dissociation}$ ) were retrieved by using Jarzynski 231 nonequilibrium equation (see Supporting Information). 27,34,35 We found  $\Delta G_{\rm dissociation}$  equal to 9.2  $\pm$  1.6, 11.6  $\pm$  0.7, and 13.4  $\pm$  0.9 kcal/mol, respectively, for the head-to-tail, head-to-head, 234 and tail-to-tail orientations (see Table S2 and Figure S13 for 235 the dissociation work histograms). It is noteworthy that each 236  $\Delta G_{
m dissociation}$  represents the combination of the  $\Delta G$  to break a cholesterol dimer and that to stretch the T40 loop (Figure 1), 238 the latter of which remains the same for all intermolecular 239 systems using the T40 loop. It is clear that the thermodynamic 240 stability of the tail-to-tail cholesterol dimer is significantly different from that of the head-to-tail or the head-to-head 242 dimers at the confidence level of 99.9% (Student's t test), 243 which is consistent with different intercholesterol contact areas 244 revealed by MD simulations above.

With this set of  $\Delta G_{\rm dissociation}$  for different cholesterol dimers, 246 we proceeded to calculate the change in free energy of 247 solubilization ( $\Delta G_{\rm solubility}$ ) of cholesterol in  $\beta$ -cyclodextrins ( $\beta$ -248 CD) or methylated  $\beta$ -CD, two well-known biomolecules for 249 cholesterol extractions. <sup>36-39</sup> By using the Hess-like cycle 250 (Figure 3),  $\Delta G_{\rm solubility}$  can be calculated in eq 1,

$$\Delta G_{\text{solubility}} = \Delta G_{\text{cholesterol dimer}} - \Delta G_{\text{host-cholesterol}} \tag{1}$$

where  $\Delta G_{ ext{cholesterol dimer}}$  is the change in free energy of 252 dissociating cholesterol dimers (either the head-tail, head- 253 head, or tail-tail orientation) and  $\Delta G_{
m host-cholesterol}$  is the free 254 energy change to dissociate host-cholesterol complex (host: 255 Me- $\beta$ CD or  $\beta$ CD). By obtaining the  $\Delta G_{\text{host-cholesterol}}$  from our 256 recent work (Figure 4A and Figure S14, here  $\Delta G_{\text{host-cholesterol}}$  257 f4 contains the  $\Delta G$  to break a host-cholesterol complex and to 258 stretch the T40 loop, the latter of which remains the same for 259 all the systems using the T40 loops), 15 we found that all 260  $\Delta G_{
m solubility}$  values of cholesterol inside the etaCDs are negative. 261 In contrast, the  $\Delta G_{\text{solubility}}$  of cholesterol in water was found to 262 be positive in the literature (5.1 kcal/mol).<sup>40</sup> These data 263 indicate that solubilization of cholesterols in  $\beta$ CD or Me- $\beta$ CD 264 is a spontaneous process. In addition, the  $\Delta G_{
m solubility}$  of 265 cholesterol in Me- $\beta$ CD (-16.05 kcal/mol) is more negative 266 than  $\beta$ CD (-8.9 kcal/mol), which is in full agreement with the 267 finding that Me- $\beta$ CD is more effective with respect to  $\beta$ CD to 268 solubilize cholesterol due to its increased size of the 269 hydrophobic cavity. Similarly, we discovered that  $\Delta G_{\text{solubility}}$  270 of the cholesterol in misaligned cholesterol dimers is more 271 negative than that in aligned cholesterol dimers (Figure 4B). 272 This result indicated that fully aligned cholesterol molecules 273 are more difficult to dissolve, which is in agreement with 274 increased IMMF for these dimers. Finally, when cholesterols 275 enter cyclodextrins with a head(hydroxyl)-on fashion, the 276 cholesterol solubility becomes larger (Figure 4B). This result 277 has been rationalized by simulations in which stronger 278 interactions persist between the hydroxy head of a cholesterol 279 and the wide opening of the cyclodextrin. 15

Bulk methods such as isothermal titration calorimetry (ITC) 281 and surface plasmon resonance (SPR) have been used to 282 investigate affinity complexes of biological molecules with 283 defined interaction orientations. However, in small molecules 284 such as cholesterols discussed here, the interactions are often 285 nonspecific without a predominant binding mode. For these 286 cases, the ensemble average approaches can only give an 287 average description of overall nonspecific interactions. Our 288 IMMF allows to precisely dissect specific interactions among 289

251

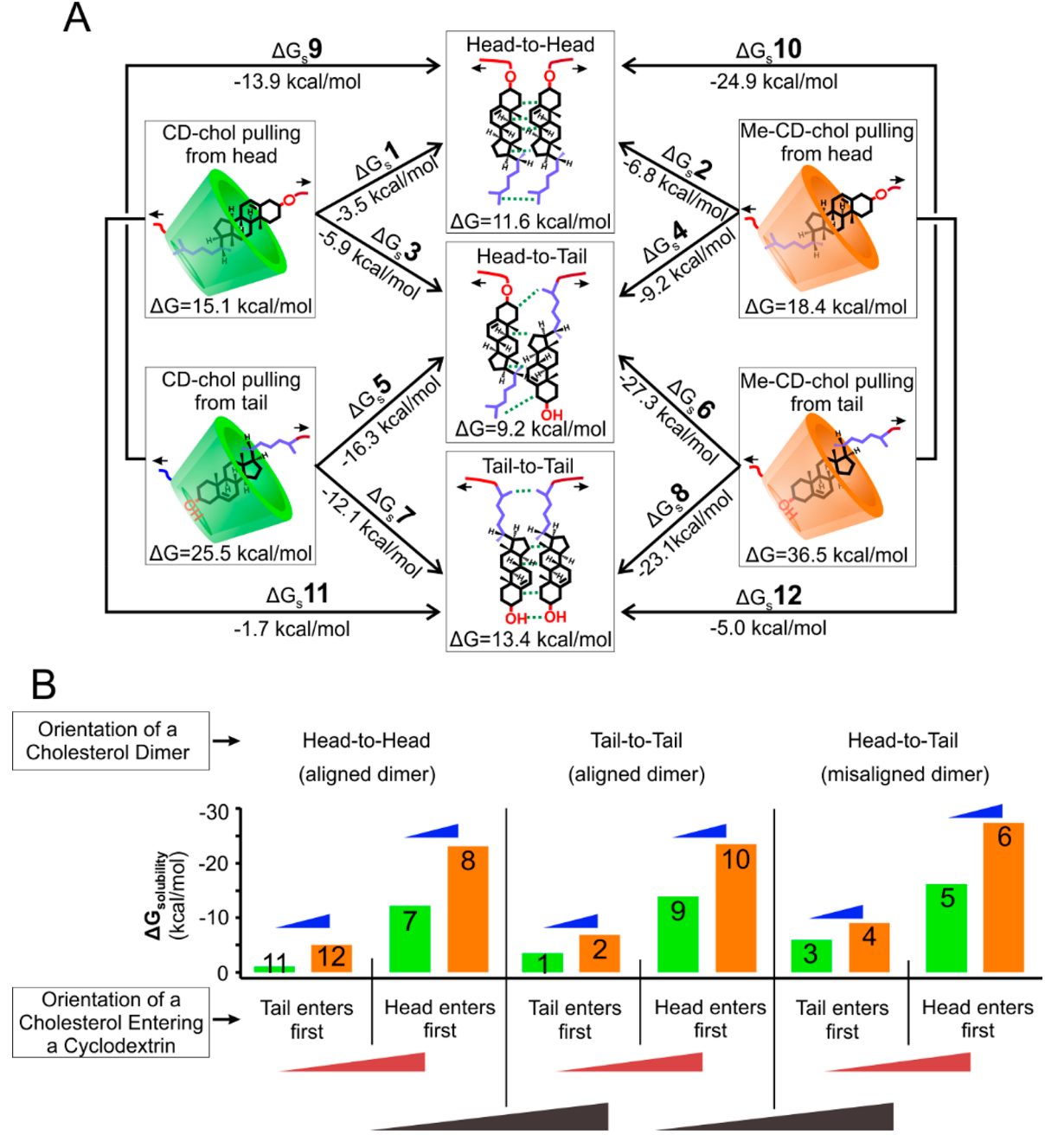


Figure 4. Summary diagram for changes in the free energy of solubilization of cholesterols in  $\beta$ CD or Me- $\beta$ CD with different interaction directions. (A) Left: Change in free energy ( $\Delta G$ ) associated with the dissociation of  $\beta$ CD-cholesterol complex pulled from the head (top) and tail (bottom) of the cholesterol (chol). Middle: Change in free energy ( $\Delta G$ ) associated with the dissociation of the cholesterol dimer pulled from the head-to-head (top), head-to-tail (middle), and tail-to-tail (bottom) orientations. Right: Change in free energy ( $\Delta G$ ) associated with the dissociation of Me- $\beta$ CD-cholesterol complex pulled from the head (top) and the tail (bottom) of the cholesterol. (B) Changes in free energy of solubilization ( $\Delta G_{\text{solubility}}$ ) of cholesterols are dependent on the disruption orientations of cholesterol—cholesterol dimers (top) as well as on the orientation of a cholesterol (bottom notation) entering either  $\beta$ -CD (green) or Me- $\beta$ -CD (brown). Slanted arrowheads depict increasing magnitudes of  $\Delta G_{\text{solubility}}$ .

290 many nonspecific binding modes, such as the head-to-head/291 tail-to-tail and the head-to-tail interacted cholesterol dimers. 292 This offers an unprecedented opportunity to understand 293 molecular interactions, such as solubilities, from a perspective 294 of defined orientations (Figure 4). 295 In conclusion, we demonstrated that the intermolecular 296 mechanical force (IMMF) can be directly measured for

In conclusion, we demonstrated that the intermolecular mechanical force (IMMF) can be directly measured for interactions between small molecules. Such IMMF indicated that fully aligned cholesterol dimers have a stronger interaction than misaligned dimers. The solubility of cholesterol in  $\beta$ CD

has been rationalized by the magnitude of IMMF, which  $_{300}$  represents a new and generic variable to describe solubility of  $_{301}$  chemicals beyond the cholesterols studied here. Given the  $_{302}$  importance of the cholesterol in various cellular and biological  $_{303}$  processes, the mechanisms of and the insights on the  $_{304}$  cholesterol dimer interaction revealed here are expected to  $_{305}$  understand a range of physiological and pathological processes involving cholesterols.

### 308 ASSOCIATED CONTENT

# 309 Supporting Information

310 The Supporting Information is available free of charge at 311 https://pubs.acs.org/doi/10.1021/acs.jpclett.1c03142.

Methods and experiments; synthesis of cholesterol functionalized DNA; Method to determine the changein-contour-length; additional figures and tables as described in the text (PDF)

#### 316 AUTHOR INFORMATION

#### 317 Corresponding Author

Hanbin Mao – Department of Chemistry and Biochemistry,
Kent State University, Kent, Ohio 44242, United States;
o orcid.org/0000-0002-6720-9429; Email: hmao@
kent.edu

#### 322 Authors

Shankar Pandey - Department of Chemistry and 323 Biochemistry, Kent State University, Kent, Ohio 44242, 324 United States; orcid.org/0000-0001-5576-6714 325 Yuan Xiang - Department of Mechanical and Aerospace 326 Engineering, The George Washington University, Washington, 327 D.C. 20052, United States; o orcid.org/0000-0002-4665-328 3360 329 Dirk Friedrich - Department of Chemistry and Biochemistry, 330 331 Kent State University, Kent, Ohio 44242, United States **Yongsheng Leng** – Department of Mechanical and Aerospace 332 Engineering, The George Washington University, Washington, 333 D.C. 20052, United States; o orcid.org/0000-0002-3558-334 335

336 Complete contact information is available at: 337 https://pubs.acs.org/10.1021/acs.jpclett.1c03142

#### 338 Notes

339 The authors declare no competing financial interest.

## **40 ACKNOWLEDGMENTS**

341 H.M. thanks prof. Janarthanan Jayawickramarajah and his 342 graduate student, Dilanka V. D. Walpita Kankanamalage from 343 Tulane University for providing 3' azido-propyl DNA during 344 the synthesis of 3' cholesterol-propyl DNA. H.M. thanks NIH 345 (R01 CA236350, for construct preparation) and NSF (CBET-346 1904921 for mechanical unfolding) for financial support. Y.L. 347 is grateful for the NSF grant (CBET-1817394) for the 348 computational studies of membrane fouling and separations.

#### 49 REFERENCES

- 350 (1) Dudko, O. K.; Hummer, G.; Szabo, A. Theory, analysis, and 351 interpretation of single-molecule force spectroscopy experiments. 352 *Proc. Natl. Acad. Sci. U. S. A.* **2008**, *105* (41), 15755–15760.
- 353 (2) Silberberg, M. S. *Principles of general chemistry*; McGraw-Hill: 354 New York, 2013.
- 355 (3) Tinoco, I.; T. X. Li, P.; Bustamante, C. Determination of 356 thermodynamics and kinetics of RNA reactions by force. *Q. Rev.* 357 *Biophys.* **2006**, 39 (4), 325–360.
- 358 (4) Evans, E. Probing the relation between force-lifetime-and 359 chemistry in single molecular bonds. *Annu. Rev. Biophys. Biomol.* 360 *Struct.* **2001**, 30, 105–28.
- (5) Moffitt, J. R.; Chemla, Y. R.; Smith, S. B.; Bustamante, C. Recent advances in optical tweezers. *Annu. Rev. Biochem.* 2008, 77, 205–228.
  (6) Mehta, A. D.; Rief, M.; Spudich, J. A.; Smith, D. A.; Simmons, R. M. Single-Molecule Biomechanics with Optical Methods. *Science* 365 1999, 283 (5408), 1689–1695.

- (7) Freikamp, A.; Cost, A.-L.; Grashoff, C. The piconewton force 366 awakens: quantifying mechanics in cells. *Trends Cell Biol.* **2016**, 26 367 (11), 838–847.
- (8) Shao, J.-Y. Measuring piconewton forces and its application in 369 cellular and molecular biomechanics. *Advances in Biomechanics* **2001**, 370 47–51.
- (9) Keller, D.; Bustamante, C. The Mechanochemistry of Molecular 372 Motors. *Biophys. J.* **2000**, 78, 541–556.
- (10) Caruso, M. M.; Davis, D. A.; Shen, Q.; Odom, S. A.; Sottos, N. 374 R.; White, S. R.; Moore, J. S. Mechanically-induced Chemical 375 Changes in Polymeric Materials. *Chem. Rev.* **2009**, *109*, 5755–5798. 376 (11) Neuman, K. C.; Nagy, A. Single-molecule force spectroscopy: 377
- optical tweezers, magnetic tweezers and atomic force microscopy. 377

  Nat. Methods 2008, 5 (6), 491–505.

  (12) Wang, L. Oian, V. Sun, V. Liu, R. Wei, G. Single melecule associated as the control of the
- (12) Wang, L.; Qian, Y.; Sun, Y.; Liu, B.; Wei, G. Single-molecule 380 force spectroscopy: A facile technique for studying the interactions 381 between biomolecules and materials interfaces. *Rev. Anal. Chem.* **2020**, 382 39 (1), 116–129.
- (13) Carrion-Vazquez, M.; Oberhauser, A. F.; Fisher, T. E.; 384 Marszalek, P.; Li, H.; Fernandez, J. M. Mechanical design of proteins 385 studied by single-molecule force spectroscopy and protein engineer- 386 ing. *Prog. Biophys. Mol. Biol.* **2000**, *74*, 63–91.
- (14) Pandey, S.; Kankanamalage, D. V. W.; Zhou, X.; Hu, C.; Isaacs, 388 L.; Jayawickramarajah, J.; Mao, H. Chaperone-Assisted Host—Guest 389 Interactions Revealed by Single-Molecule Force Spectroscopy. J. Am. 390 Chem. Soc. 2019, 141 (46), 18385—18389.
- (15) Pandey, S.; Xiang, Y.; Walpita Kankanamalage, D. V. D.; 392 Jayawickramarajah, J.; Leng, Y.; Mao, H. Measurement of Single- 393 Molecule Forces in Cholesterol and Cyclodextrin Host–Guest 394 Complexes. J. Phys. Chem. B 2021, 125 (40), 11112–11121.
- (16) Ramamoorthy, S.; Cidlowski, J. A. Corticosteroids: Mecha- 396 nisms of Action in Health and Disease. *Rheum Dis Clin North Am.* 397 **2016**, 42 (1), 15–vii. 398
- (17) Berg, J.; Tymoczko, J.; Stryer, L. Important derivatives of 399 cholesterol include bile salts and steroid hormones. *Biochemistry*, 5th 400 ed.; WH Freeman: New York, 2002; section 26.4.
- (18) Elkins, M. R.; Bandara, A.; Pantelopulos, G. A.; Straub, J. E.; 402 Hong, M. Direct Observation of Cholesterol Dimers and Tetramers in 403 Lipid Bilayers. J. Phys. Chem. B **2021**, 125 (7), 1825–1837.
- (19) Hung, W.-C.; Lee, M.-T.; Chen, F.-Y.; Huang, H. W. The 405 Condensing Effect of Cholesterol in Lipid Bilayers. *Biophys. J.* **2007**, 406 92 (11), 3960–3967.
- (20) Miao, L.; Nielsen, M.; Thewalt, J.; Ipsen, J. H.; Bloom, M.; 408 Zuckermann, M. J.; Mouritsen, O. G. From Lanosterol to Cholesterol: 409 Structural Evolution and Differential Effects on Lipid Bilayers. 410 *Biophys. J.* **2002**, 82 (3), 1429–1444.
- (21) Simons, K.; Toomre, D. Lipid rafts and signal transduction. 412 *Nat. Rev. Mol. Cell Biol.* **2000**, *1* (1), 31–39.
- (22) Tewary, P.; Veena, K.; Pucadyil, T. J.; Chattopadhyay, A.; 414 Madhubala, R. The sterol-binding antibiotic nystatin inhibits entry of 415 non-opsonized Leishmania donovani into macrophages. *Biochem.* 416 *Biophys. Res. Commun.* **2006**, 339 (2), 661–666.
- (23) Kumar, G. A.; Jafurulla, M.; Chattopadhyay, A. The membrane 418 as the gatekeeper of infection: Cholesterol in host-pathogen 419 interaction. *Chem. Phys. Lipids* **2016**, *199*, 179–185.
- (24) Silvius, J. R. Role of cholesterol in lipid raft formation: lessons 421 from lipid model systems. *Biochim. Biophys. Acta, Biomembr.* **2003**, 422 *1610* (2), 174–183.
- (25) Varsano, N.; Beghi, F.; Elad, N.; Pereiro, E.; Dadosh, T.; 424 Pinkas, I.; Perez-Berna, A. J.; Jin, X.; Kruth, H. S.; Leiserowitz, L.; 425 Addadi, L. Two polymorphic cholesterol monohydrate crystal 426 structures form in macrophage culture models of atherosclerosis. 427 *Proc. Natl. Acad. Sci. U. S. A.* **2018**, *115* (30), 7662–7669.
- (26) Dhakal, S.; Yu, Z.; Konik, R.; Cui, Y.; Koirala, D.; Mao, H. G- 429 Quadruplex and i-Motif Are Mutually Exclusive in ILPR Double- 430 Stranded DNA. *Biophys. J.* 2012, 102 (June), 2575–2584.
- (27) Yu, Z.; Schonhoft, J. D.; Dhakal, S.; Bajracharya, R.; Hegde, R.; 432 Basu, S.; Mao, H. ILPR G-Quadruplexes Formed in Seconds 433

- 434 Demonstrate High Mechanical Stabilities. J. Am. Chem. Soc. 2009, 131 435 (5), 1876–1882.
- 436 (28) Koirala, D.; Dhakal, S.; Ashbridge, B.; Sannohe, Y.; Rodriguez,
- 437 R.; Sugiyama, H.; Balasubramanian, S.; Mao, H. A Single-Molecule
- 438 Platform for Investigation of Interactions between G-quadruplexes 439 and Small-Molecule Ligands. *Nat. Chem.* **2011**, *3*, 782–787.
- 440 (29) Woodside, M. T.; Behnke-Parks, W. M.; Larizadeh, K.; Travers,
- 441 K.; Herschlag, D.; Block, S. M. Nanomechanical measurements of the
- 442 sequence-dependent folding landscapes of single nucleic acid hairpins.
- 443 Proc. Natl. Acad. Sci. U. S. A. 2006, 103 (16), 6190-6195.
- 444 (30) Kolb, H. C.; Finn, M. G.; Sharpless, K. B. Click Chemistry:
- 445 Diverse Chemical Function from a Few Good Reactions. Angew.
- 446 Chem., Int. Ed. 2001, 40, 2004-2021.
- 447 (31) Park, S.; Khalili-Araghi, F.; Tajkhorshid, E.; Schulten, K. Free 448 energy calculation from steered molecular dynamics simulations using
- 449 Jarzynski's equality. J. Chem. Phys. 2003, 119 (6), 3559-3566.
- 450 (32) Park, S.; Schulten, K. Calculating potentials of mean force from 451 steered molecular dynamics simulations. *J. Chem. Phys.* **2004**, 120
- 452 (13), 5946-5961.
- 453 (33) Makarov, D. E. Communication: Does force spectroscopy of 454 biomolecules probe their intrinsic dynamic properties? *J. Chem. Phys.*
- 455 **2014**, 141 (24), 241103.
- 456 (34) Jarzynski, C. Nonequilibrium Equality for Free Energy
- 457 Differences. Phys. Rev. Lett. 1997, 78, 2690-2693.
- 458 (35) Liphardt, J.; Dumont, S.; Smith, S. B.; Tinoco, I., Jr.;
- 459 Bustamante, C. Equilibrium information from nonequilibrium 460 measurements in an experimental test of Jarzynski's equality. *Science*
- 461 **2002**, 296 (5574), 1832–1835.
- 462 (36) Irie, T.; Otagiri, M.; Sunada, M.; Uekama, K.; Ohtani, Y.;
- 463 Yamada, Y.; Sugiyama, Y. Cyclodextrin-induced hemolysis and shape
- 464 changes of human erythrocytes in vitro. J. Pharmacobio-Dyn. 1982, 5 465 (9), 741–744.
- 466 (37) Zimmer, S.; Grebe, A.; Bakke, S. S.; Bode, N.; Halvorsen, B.;
- 467 Ulas, T.; Skjelland, M.; De Nardo, D.; Labzin, L. I.; Kerksiek, A.;
- 468 Hempel, C.; Heneka, M. T.; Hawxhurst, V.; Fitzgerald, M. L.;
- 469 Trebicka, J.; Björkhem, I.; Gustafsson, J.-Å.; Westerterp, M.; Tall, A.
- 470 R.; Wright, S. D.; Espevik, T.; Schultze, J. L.; Nickenig, G.; Lütjohann,
- 471 D.; Latz, E. Cyclodextrin promotes atherosclerosis regression via 472 macrophage reprogramming. Sci. Transl. Med. 2016, 8 (333), 333ra50.
- 473 (38) Kim, H.; Han, J.; Park, J.-H. Cyclodextrin polymer improves
- 474 atherosclerosis therapy and reduces ototoxicity. J. Controlled Release
- 475 **2020**, 319, 77-86.
- 476 (39) Beseničar, M. P.; Bavdek, A.; Kladnik, A.; Maček, P.; Anderluh,
- 477 G. Kinetics of cholesterol extraction from lipid membranes by methyl-
- 478  $\beta$ -cyclodextrin—A surface plasmon resonance approach. *Biochim.*
- 479 Biophys. Acta, Biomembr. 2008, 1778 (1), 175-184.
- 480 (40) Bux, K.; Moin, S. T. Solvation of cholesterol in different
- 481 solvents: a molecular dynamics simulation study. Phys. Chem. Chem.
- 482 Phys. **2020**, 22 (3), 1154-1167.